inorganics

MDPI

Article

Controlled Synthesis of Alkali Metal Hydroxide Particles via Solvothermal Processing

Chiara Tuccio [1,2], Francesco Armetta [1,3,*], Delia Francesca Chillura Martino [1], Ramūnas Skaudžius [4] and Maria Luisa Saladino [1,3,*]

1 Department of Biological, Chemical and Pharmaceutical Sciences and Technologies (STEBICEF), University of Palermo, Viale delle Scienze, Bld.17, I-90128 Palermo, Italy; chiara.tuccio@unipa.it (C.T.); delia.chilluramartino@unipa.it (D.F.C.M.)
2 Department of Cultures and Societies, University of Palermo, Viale delle Scienze, Bld.15, I-90128 Palermo, Italy
3 Consiglio Nazionale Delle Ricerche, Istituto per i Processi Chimico Fisici, CNR-IPCF-Messina, Viale Ferdinando Stagno d'Alcontres 37, I-98158 Messina, Italy
4 Institute of Chemistry, Faculty of Chemistry and Geosciences, Vilnius University, Naugarduko 24, LT–03225 Vilnius, Lithuania; ramunas.skaudzius@chgf.vu.lt
* Correspondence: francesco.armetta01@unipa.it (F.A.); marialuisa.saladino@unipa.it (M.L.S.)

Abstract

This study presents a solvothermal approach starting from micron-sized hydroxide precursors, which combines features of top-down size reduction and bottom-up recrystallization, leading to nanoscale hydroxide particles. The method is based on autoclave treatment at a moderate temperature (180 °C) and a pressure of 8 bar, using different mixtures of water and isopropanol. The hydroxide precursors, used in micrometric form without surfactants or additives, were converted into nanoscale particles through a one-pot, one-step process. The nanomaterials obtained were characterized using X-ray diffraction (XRD), Fourier transform infrared spectroscopy (FTIR), optical microscopy (MO), scanning electron microscopy (SEM), transmission electron microscopy (TEM) and Brunauer–Emmett–Teller (BET) surface area analysis to assess their structural, morphological and textural characteristics. The results show that solvent composition and precursor concentration strongly influence the crystalline phase, particle morphology, dispersion stability and surface area. Well-defined acicular and fibrous morphologies were obtained for $Ba(OH)_2$ and $Sr(OH)_2$, while $Mg(OH)_2$ formed spherical and hexagonal structures, respectively. Of all the conditions tested, the 75:25 water/isopropanol ratio produced the most stable systems. This work provides a method to produce alkaline earth hydroxide nanoparticles with tunable properties.

Keywords: solvothermal synthesis; hydroxide nanoparticles; barium; magnesium; strontium; top-down approach; autoclave; particle morphology; needles

check for updates

Academic Editors: Torben R. Jensen, Eleonora Aneggi, Roberto Nisticò and Hicham Idriss

Received: 10 October 2025
Revised: 2 November 2025
Accepted: 7 November 2025
Published: 9 November 2025

Citation: Tuccio, C.; Armetta, F.; Chillura Martino, D.F.; Skaudžius, R.; Saladino, M.L. Controlled Synthesis of Alkali Metal Hydroxide Particles via Solvothermal Processing. *Inorganics* **2025**, *13*, 373. https://doi.org/10.3390/inorganics13110373

Copyright: © 2025 by the authors. Licensee MDPI, Basel, Switzerland. This article is an open access article distributed under the terms and conditions of the Creative Commons Attribution (CC BY) license (https://creativecommons.org/licenses/by/4.0/).

1. Introduction

The controlled production of nanomaterials has become a central topic in materials chemistry [1,2], due to the ability to finely modulate particle size, morphology, crystallinity, and surface properties. Nanoparticles, particularly those composed of alkaline earth metal hydroxides such as barium, magnesium, and strontium, are increasingly employed in a wide range of applications [3–5], from catalysis and environmental remediation to biomedicine, advanced materials, and more recently, cultural heritage conservation.

Synthesis strategies for nanoparticles generally fall into two main categories: bottom-up and top-down approaches [6,7]. The bottom-up (chemical) method, also referred to as

"molecular nanotechnology," involves the growth of nanostructures through the assembly of atoms or molecules, allowing for controlled development from molecular precursors [8]. The top-down (physical) approach, by contrast, achieves nanoscale dimensions by reducing bulk materials into smaller particles, using mechanical, chemical, or other forms of energy [9].

Despite the growing interest in alkaline earth metal hydroxides, currently available synthesis methods often present several limitations, including operational complexity, the use of toxic solvents, or the need for stabilizing agents.

For instance, magnesium hydroxide nanoparticles can be obtained via simple hydrothermal synthesis using magnesium salts and urea, yielding flower-like structures of stacked nanosheets [10]. Alternatively, reverse microemulsion methods enable precise control over particle size, producing monodisperse and hydrophobic nanoparticles ideal for nonpolar media [11]. Or they can be obtained by homogeneous chemical precipitation from aqueous solutions containing magnesium salts (chloride, nitrate, sulfate, perchlorate) and sodium hydroxide as precipitating agents [12].

The synthesis of barium hydroxide nanoparticles is limited by their high solubility in water, which makes the bottom-up approach difficult. An effective alternative is a top-down method, in which micrometer-sized crystals of $Ba(OH)_2$ are ground in short-chain alcohols (1- or 2-propanol) under high temperature and pressure, resulting in particles of about 100 nm [13].

Strontium hydroxide synthesis also suffers from limitations related to water solubility. However, homogeneous-phase protocols at low temperatures have been described, employing simple commercial salts ($Sr(NO_3)_2$ and NaOH) under controlled conditions. This process allows for the production of nearly spherical $Sr(OH)_2$ particles with sizes around 30 nm. Although these approaches have led to promising results, many still require extended purification phases and complex equipment or are difficult to scale up [14].

Among the most promising top-down techniques is hydrothermal synthesis [15], which enables the direct formation of crystalline phases in aqueous or mixed-solvent media under an elevated temperature and pressure. Hydrothermal or solvothermal treatments in autoclaves are particularly attractive due to their ability to generate high-purity, crystalline materials without intermediate calcination or sintering steps. Moreover, the use of green solvents such as water and short-chain alcohols (e.g., ethanol, isopropanol) reduces toxicity and improves particle dispersion in the final colloidal systems.

This work presents a one-pot, one-step solvothermal route for the efficient and reproducible synthesis of barium, magnesium, and strontium hydroxide nanoparticles. The novelty of this work lies in combining a mixed-solvent system (water/isopropanol) with a solvothermal process starting from bulk precursors, enabling nanoparticle formation without surfactants or complex purification steps. The methodology relies solely on simple and commercially available precursors combined with non-toxic solvents (water and isopropanol) in varying proportions. Isopropanol and 1-propanol (the latter for comparison testing) were chosen as solvents because they have already been used successfully in previous solvothermal syntheses of alkaline earth metal hydroxides [13]. The synthesis is carried out in sealed autoclaves at moderate temperatures (up to 180 °C), without the addition of surfactants, chelating agents, or other auxiliaries.

In response to current challenges in sustainable nanomaterial production, we report a new method for synthesizing alkaline earth metal hydroxide nanoparticles. This approach is environmentally friendly and economically viable, as it avoids the use of hazardous chemicals and complex purification steps. The influence of synthesis parameters—such as precursor concentration and solvent ratio—on particle morphology and size was systematically investigated. The resulting materials were characterized using X-ray diffraction (XRD),

Fourier-transform infrared spectroscopy (FTIR), optical microscopy, scanning electron microscopy (SEM), transmission electron microscopy (TEM), and nitrogen gas adsorption.

2. Results and Discussion

A summary of the obtained particles in different conditions is shown in Table 1.

Table 1. Synthesis conditions and obtained products at 180 °C, 8 hPa, 24 h.

Label	Type	Solvent	Concentration (mol/L)	Aspect	Particles	Composition
CT1	$Ba(OH)_2$	water	0.099	particles in suspension	powder	$Ba(OH)_2$ and $BaCO_3$
CT2	$Ba(OH)_2$	isopropanol	0.099	colloidal solution	powder	$Ba(OH)_2$
CT3	$Ba(OH)_2$	1-propanol	0.099	precipitate	powder	$Ba(OH)_2$
CT4	$Ba(OH)_2$	water/isopropanol = 25:75	0.025	unstable milky colloidal solution	powder and crystals	$Ba(OH)_2$
CT5	$Ba(OH)_2$	water/isopropanol = 75:25	0.070	stable colloidal solution for 1 h	crystals	$Ba(OH)_2$
CT6	$Ba(OH)_2$	water/isopropanol = 50:50	0.050	unstable colloidal solution	powder	$Ba(OH)_2$
CT7	$Ba(OH)_2$	water in presence nitrogen	0.099	particles in suspension	powder	$Ba(OH)_2$ and $BaCO_3$
SR1	$Sr(OH)_2$	water/isopropanol = 75:25	0.148	stable milky colloidal solution for 1 h	crystals	$Sr(OH)_2$
MG1	$Mg(OH)_2$	water/isopropanol = 75:25	0.017	stable colloidal solution for 1 h	powder	$Mg(OH)_2$

Regarding the synthesis of $Ba(OH)_2$ particles, their composition and stability are affected by the used solvent. In all experiments, the total solvent volume was kept constant at 50 mL, while only the solvent type and the percentage ratio were varied. The product obtained by using water as a solvent was a mixture of hydroxides and carbonates, also insufflating nitrogen. The product obtained by using 1-propanol as a solvent was hydroxide, but the dispersion was not stable. The particles obtained by using a mixture of water and isopropanol gave the best results in terms of composition and stability. In detail, the most stable dispersion was obtained with a 75% water and 25% isopropanol mixture. Based on these promising results for $Ba(OH)_2$, the same synthetic methodology, solvent types, and solvent ratio were applied to the preparation of $Sr(OH)_2$ and $Mg(OH)_2$. All dispersions showed good stability under the same conditions. The stability of the dispersions was first assessed qualitatively through visual observation over time, monitoring the appearance of turbidity or sedimentation. Under these conditions, the systems remained macroscopically stable for approximately one hour at room temperature, with the best performance observed for the 75:25 water/isopropanol mixture. Although qualitative, these observations were reproducible across multiple preparations, confirming the enhanced colloidal stability achieved under these solvent conditions. To further evaluate dispersion stability, turbidimetric measurements were carried out. The absorbance of the dispersions remained unchanged for 60 min, indicating stability within this time range. Moreover, after gentle agitation, the dispersions appeared homogeneous, and the Tyndall effect was clearly visible when illuminated with a red laser, further confirming their colloidal nature (inset in Figure 1).

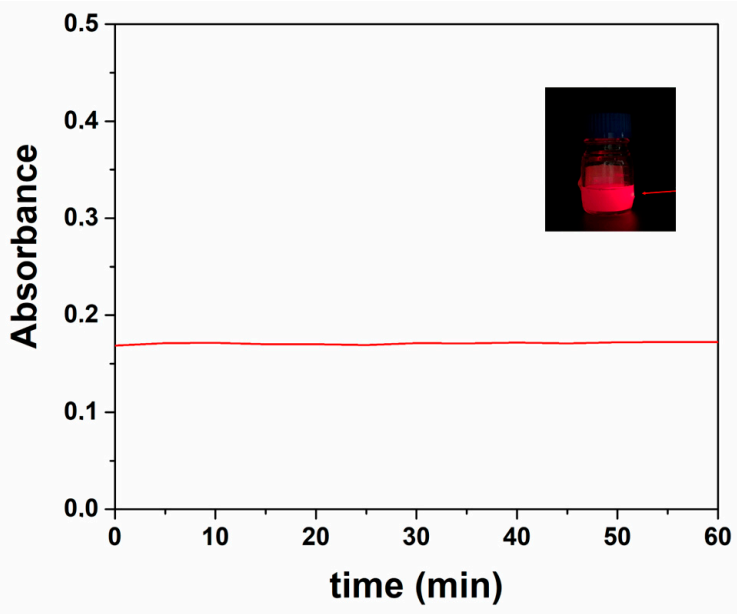

Figure 1. Absorbance of the dispersion monitored for 60 min. Tyndall effect observed in the $Sr(OH)_2$ dispersion under red laser illumination. The arrow indicates the laser beam path through the dispersion.

For the above findings, here we report the characterization of the three samples prepared in 75% water and 25% isopropanol mixture ($Mg(OH)_2$ = MG1, $Sr(OH)_2$ = SR1, $Ba(OH)_2$ = CT5).

The XRD patterns of the powders show the crystalline phases formed under autoclave synthesis conditions (Figure 2). MG1 exhibits characteristic peaks corresponding to the brucite phase (magnesium hydroxide, $Mg(OH)_2$ ref code 01-074-2220) with a hexagonal crystal system. SR1 is identified as strontium hydroxide octahydrate ($Sr(OH)_2{\cdot}8H_2O$ ref code 00-027-1438), with a tetragonal crystal system, where the (202) peak appears more intense and broader. Similarly, CT5 corresponds to barium hydroxide octahydrate ($Ba(OH)_2{\cdot}8H_2O$ ref code 01-076-0916), crystallized in a monoclinic system. The autoclave synthesis promotes the formation of hydrated hydroxide phases for strontium and barium, as the controlled temperature and pressure conditions favored water incorporation into their crystalline structures. In the case of magnesium, the small ionic radio of the cation likely mitigates the incorporation of water. The FTIR spectra of the synthesized compounds for different metals exhibit three similar profiles. All spectra show a broad absorption band in the range around 3000 cm^{-1}, assigned to the O–H stretching vibration of hydroxyl groups. The absence of characteristic carbonate bands indicates that no CO_3^{2-} species were formed during the solvothermal treatment, in agreement with the XRD results that confirmed the exclusive presence of hydroxide phases. In the low-wavenumber region (<600 cm^{-1}), bands corresponding to M–O and M–OH lattice vibrations (where M = Ba, Sr, or Mg) are observed, further confirming the formation of crystalline hydroxide structures.

According to XRD patterns, the absence of carbonate bands indicates that the synthesis in the above solvent in the autoclave favored the stabilization of hydroxide phases without carbonate formation.

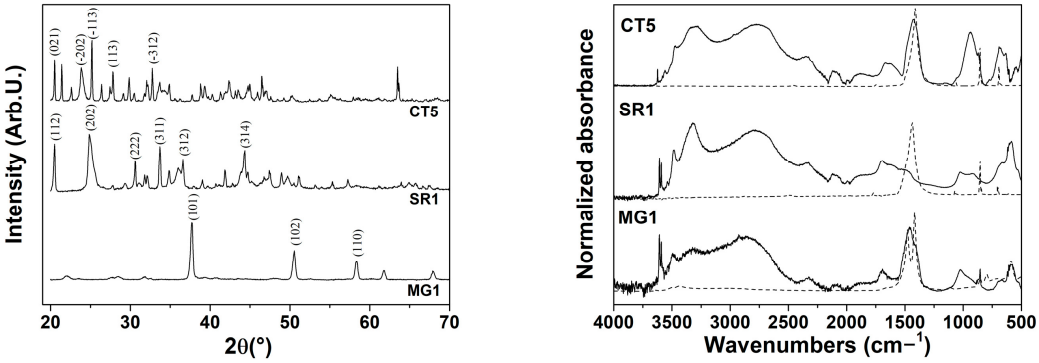

Figure 2. (**left**) XRD patterns and (**right**) FTIR spectra of $Mg(OH)_2$, $Sr(OH)_2$ and $Ba(OH)_2$ compounds obtained by the hydrothermal synthesis ($Mg(OH)_2$ = MG1, $Sr(OH)_2$ = SR1, $Ba(OH)_2$ = CT5).

In addition, the acicular crystals typical of barium hydroxide and strontium hydroxide were observed in SEM images (Figure 3) in the dispersions prepared with 75% water and 25% isopropanol and a homogeneous particle distribution. On the contrary, for magnesium hydroxide (MG1 sample), no characteristic morphology was visible macroscopically; further details were observed under the optical microscope. The barium hydroxide (CT5) and strontium hydroxide (SR1) samples showed particles with both acicular and cubic shape with nanometric dimensions. These cubic crystals suggest that controlled crystallization is favored by the solvent mixtures. The magnesium hydroxide (MG1) particles show homogeneous and spherical distribution.

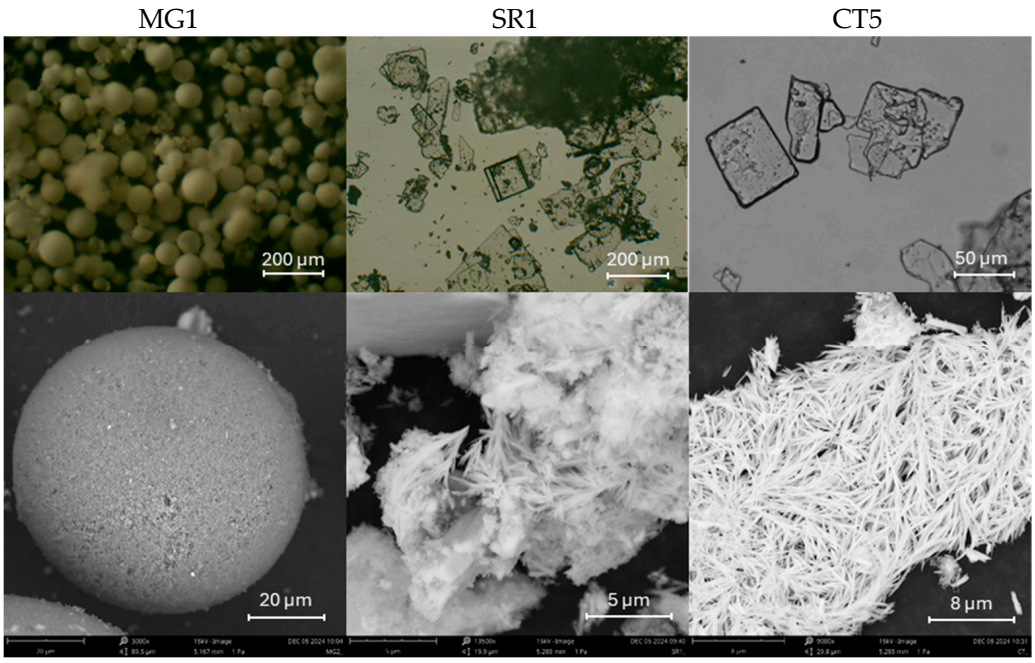

Figure 3. (**up**) Images obtained under the optical microscope (OM)OM; (**down**) SEM micrographs of MG1, SR1 and CT5 samples.

SEM observations confirmed the similarities found for the barium hydroxide (CT5) and strontium hydroxide (SR1) samples, which are characterized by a fibrous structure. A perfectly delineated spherical shape is observed for the magnesium hydroxide (MG1) samples, whose particle size distribution is reported in Figure 4. From the graph, it can be seen that the particles range in size from around 60 µm to 290 µm.

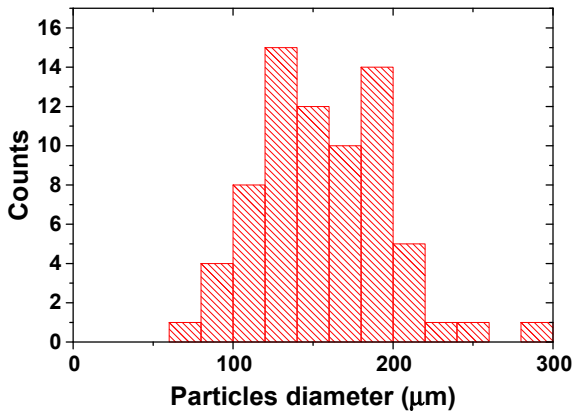

Figure 4. Particle size distribution for $Mg(OH)_2$ particles, obtained by OM images.

The TEM micrographs (Figure 5) of the CT5 sample show three different morphologies of barium hydroxide particles. Type 2 and 3 structures show a marked acicular morphology, which is typical for barium hydroxide: in type 2 structures, well-defined needles arranged in a radial pattern are observed, while in type 3 structures, bundles of flexible nanocrystals are formed. Type 1, on the other hand, shows disordered aggregates of nanosheets, indicative of a less oriented growth. The observed morphological variety reflects the influence of the synthesis conditions on the structural development of the material.

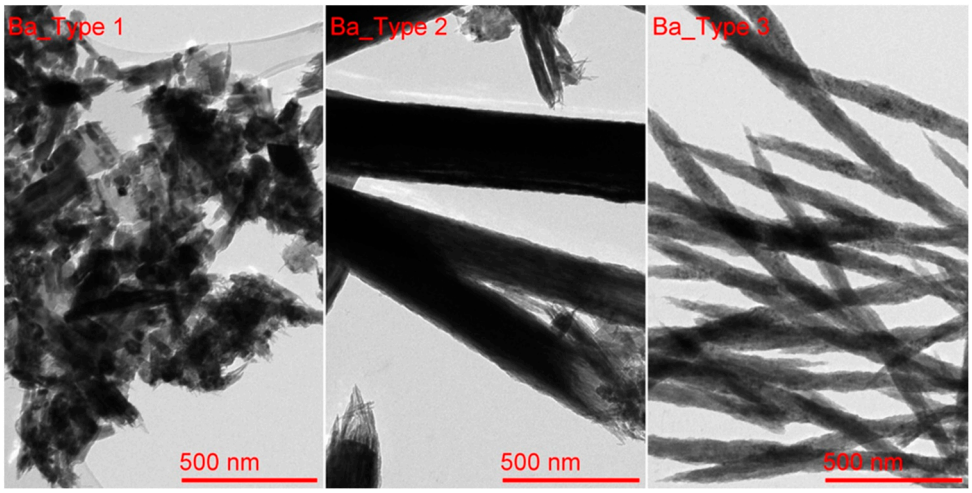

Figure 5. TEM micrographs of CT5 sample.

Micrographs analysis (Table 2) supports the morphological distinctions among the three barium hydroxide particle types. Type 2 exhibits the highest average length (~163 nm) and area (~121 nm^2), consistent with the formation of well-defined, radially arranged needle-like crystals. The large standard deviation in length and area also indicates significant dimensional variability, likely due to differences in needle growth or partial overlap. Type 3 structures, although shorter (~53 nm), are characterized by higher pixel intensities, reflecting denser or thicker nanocrystals arranged in bundled configurations. In contrast, Type 1 shows the smallest dimensions (mean length ~50 nm, area ~51 nm^2) and a more moderate intensity range, in line with its morphology of disordered nanosheets. These quantitative differences confirm that the synthesis conditions result in markedly distinct crystallization pathways, influencing not only the shape but also the size distribution and density of the resulting particles.

TEM micrographs (Figure 6-up) of MG1 sample show magnesium hydroxide particles. The sample exhibits a relatively homogeneous morphology, consisting mainly of

overlapping lamellar structures accompanied by well-defined hexagonal particles. The coexistence of plates and hexagonal shapes suggests controlled growth along preferential crystallographic planes, influenced by the hydrothermal conditions of synthesis.

Table 2. Analysis of particle morphology from TEM micrographs of CT5 sample.

			CT5 Type 1			
Label	Area	Mean	Min	Max	Angle	Lenght
Mean	50.967	74.845	58.235	118.942	−53.685	49.98
SD	14.485	37.161	32.813	56.004	82.66	14.538
Min	30	18.565	14.91	30	−165.5	29
Max	77	160.855	144.093	241.136	175.236	76.485
			CT5 Type 2			
Label	Area	Mean	Min	Max	Angle	Lenght
Mean	121.088	48.872	29.815	156.531	−67.419	162.673
SD	70.634	22.027	18.928	61.880	56.562	95.338
Min	22.488	16.214	5.054	61.000	−145.491	29.624
Max	217.750	105.665	77.000	255.000	14.931	293.412
			CT5 Type 3			
Label	Area	Mean	Min	Max	Angle	Lenght
Mean	39.491	115.408	89.863	168.329	−85.771	52.615
SD	13.88	28.427	28.341	40.109	54.933	18.747
Min	18.1	60.057	43.927	92	−175.236	23.884
Max	67.464	164.805	144.796	254.667	20.323	90.68

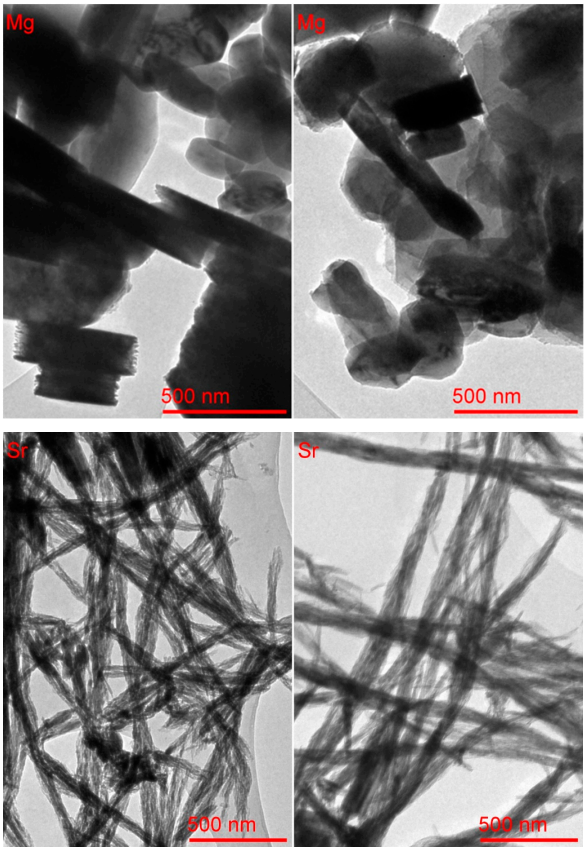

Figure 6. TEM micrographs of MG1 (**up**) and SR1 samples (**down**).

The images of micrographs (Table 3) confirm the relatively uniform size and shape distribution of magnesium hydroxide particles, despite local morphological variations observable in different regions of the same sample. The measured mean particle area is approximately 200–225 nm^2, with average lengths ranging from 139 to 157 nm. The standard deviations, particularly in the second image region, indicate moderate polydispersity, likely due to overlapping or aggregation effects. Notably, the pixel intensity is lower in the second region, suggesting a local decrease in thickness or electron density, possibly associated with differences in the stacking or orientation of lamellar structures. Overall, the data support the interpretation of a homogeneous material composed of plate-like and hexagonal particles with a controlled crystallization pattern.

Table 3. Analysis of particle morphology from TEM micrographs of MG1 sample.

MG1 (image left)						
Label	Area	Mean	Min	Max	Angle	Lenght
Mean	199.556	59.086	45.028	116.717	−100.87	139.199
SD	51.374	29.015	23.948	59.915	36.37	36.257
Min	96.787	27.325	23.961	42.713	−170.074	66.981
Max	360.936	158.205	135.354	255	−25.074	252.955
MG1 (image right)						
Label	Area	Mean	Min	Max	Angle	Lenght
Mean	225.702	40.944	27.241	81.298	−85.167	157.486
SD	107.575	25.117	22.143	46.628	41.144	75.625
Min	118.968	5.009	0	14	−147.171	82.958
Max	594.838	107.997	91.71	215	−3.521	416.796

The TEM micrographs (Figure 6-down) of the SR1 sample show strontium hydroxide particles. The sample shows a homogeneous morphology characterized by thin, elongated acicular structures intertwined to form fibrillar bundles and networks. This arrangement suggests marked anisotropic growth typical of strontium hydroxide, favored by the hydrothermal synthesis conditions. Micrograph analysis (Table 4) supports the morphological homogeneity observed in the TEM micrographs. Both regions of the $Sr(OH)_2$ sample exhibit similar characteristics, with elongated particles forming fibrous networks. The average particle length increases from ~66 nm in the left region to ~91 nm in the right, accompanied by a wider dispersion (SD ~32 nm), indicating variability in bundle thickness and possible overlap. The higher mean area in the second region (~166 nm^2) also suggests denser or more bundled nanofibers. Pixel intensity values are consistent across both regions, with moderate variation, reflecting relatively uniform density or thickness among the fibrils. The narrow angular distributions further support the aligned, interwoven structure of the acicular aggregates, typical of anisotropic crystal growth under hydrothermal conditions. The morphological differences observed among $Ba(OH)_2$, $Sr(OH)_2$, and $Mg(OH)_2$ particles are mainly related to the different chemical natures and solubilities of the cations, which affect the nucleation and growth processes during the solvothermal treatment. The solvent composition also plays a role, as the mixed water/isopropanol system can influence surface energy and crystal growth direction, leading to the formation of distinct shapes such as acicular, plate-like, or spherical particles.

Table 4. Analysis of particle morphology from TEM images of SR1 sample.

SR1 (image left)						
Label	Area	Mean	Min	Max	Angle	Lenght
Mean	120.638	101.344	69.482	164.1	−89.693	65.584
SD	38.842	31.937	25.643	43.278	70.48	21.576
Min	67.738	17.917	8	31	−173.157	35.559
Max	232.244	141.83	108.086	218.638	15.642	128.071
SR1 (image right)						
Label	Area	Mean	Min	Max	Angle	Lenght
Mean	165.904	94.001	69.293	155.544	−100.689	90.622
SD	57.631	30.005	25.698	52.173	41.601	32.11
Min	103.22	14.756	7	44	−163.301	56.109
Max	322.562	155.239	123.333	232	−26.565	177.867

Nitrogen adsorption–desorption measurements provided insight into the specific surface area and porosity of the hydroxide samples (Table 5). Among the three samples, MG1 exhibited the highest BET surface area, with a value of 14.55 ± 0.03 m^2/g, indicative of a well-developed porous structure. SR1 presented an intermediate surface area of 5.18 ± 0.09 m^2/g, while CT5 showed a markedly lower value of 2.52 ± 0.06 m^2/g, suggesting a more compact morphology or greater degree of particle aggregation. The average pore diameters also varied considerably: CT5 featured the largest pores (14.24 nm), followed by SR1 (11.35 nm) and MG1 (9.85 nm). These values suggest that MG1 possesses a more finely structured mesoporous framework, which correlates well with its lamellar morphology observed in TEM images. Conversely, the low surface area yet larger pore size in CT5 may be attributed to the formation of dense or aggregated needle-like structures. SR1's intermediate values in both parameters likely reflect its fibrillar morphology with moderate porosity and structural openness.

Table 5. BET analysis results: specific surface area and average pore diameter.

Sample	**BET Surface Area, m^2/g**	**Average Pore Size, nm**
SR1	5.178 ± 0.09	11.3
MG1	14.55 ± 0.03	9.8
CT5	2.52 ± 0.06	14.2

These results highlight how optimized synthesis conditions, particularly the use of a water/isopropanol solvent system and moderate solvothermal parameters, favor the controlled growth of crystalline hydroxide structures and the formation of stable, well-defined nanoparticles. The strong correlation between particle morphology (as observed by TEM) and surface area/porosity (from BET analysis) confirms the reliability and reproducibility of the proposed one-pot method. In general, different morphologies of hydroxide particles arise from the combined influence of thermodynamic and kinetic factors during nucleation and growth. In particular, the solvent composition, precursor concentration, temperature, and intrinsic solubility of each hydroxide play crucial roles. The solvent (water/alcohol ratio) affects the dielectric constant and polarity of the medium, modifying ion solvation and the supersaturation level, which in turn govern nucleation and crystal growth rates. Moreover, the different solubilities of $Ba(OH)_2$, $Sr(OH)_2$, and $Mg(OH)_2$ lead to distinct

precipitation kinetics: the less soluble hydroxides tend to nucleate rapidly, producing smaller and less ordered particles, while the more soluble species undergo slower growth and recrystallization, forming larger or more defined morphologies. In addition, alcohol molecules may selectively adsorb onto specific crystal faces, influencing anisotropic growth and further contributing to morphological diversity.

The final stages involved filtering and drying the resulting solution to obtain the particles in powder form. The particles were dispersed (Figure 7) in different solvents in order to obtain a dispersed system that is stable over time. The particles obtained in powder form were redispersed in water, isopropanol, and a water/isopropanol mixture (75:25), with the aim of evaluating the best dispersion system. To improve the stability and homogeneity of the system, the dispersions were sonicated in an ultrasonic bath for 30 min.

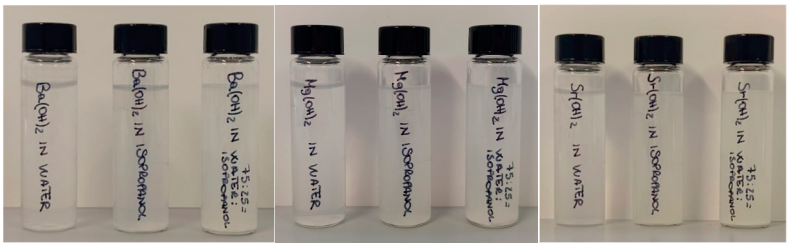

Figure 7. Redispersion of hydroxide in water, isopropanol, and 75:25 water/isopropanol mixture.

The results showed that the dispersions remained stable for about 1 h, with the best performance observed in the water/isopropanol mixture (75:25) for the same percentages used for hydrothermal synthesis. Compared to previously documented approaches, which were often characterized by bottom-up, multi-step synthesis and the use of multiple precursors, the methodology developed in this work is distinguished by the use of a top-down approach, simplifying the process and making it more efficient and sustainable. The use of isopropanol has also been explored in other studies, but an important optimization is reported here due to the reduction in the amount of alcohol used. This choice not only reduces the overall toxicity of the process but also allows for lower production costs.

3. Materials and Methods

3.1. Materials

All the chemical reagents and solvents used in this work were supplied by Sigma Aldrich: technical-grade barium hydroxide ($Ba(OH)_2$), technical-grade ~95% strontium hydroxide ($Sr(OH)_2$), ~94% magnesium hydroxide ($Mg(OH)_2$) from BioUltra at ≥99.0% (KT), isopropyl alcohol at ≥99.7%, FCC, FG, and 1-propanol. Deionized water was prepared with an ionized water purification system (Demineraliser model minidem, CTS conservation) and was used in all procedures.

3.2. Synthesis of Barium, Strontium, and Magnesium Hydroxide Nanoparticles

Barium, strontium, and magnesium hydroxide were synthesized using the solvothermal method using $Ba(OH)_2$, Sr $(OH)_2$, and $Mg(OH)_2$ at micrometer sizes as reagents and different solvents. The concentrations of barium hydroxide and strontium hydroxide were set according to their solubility limit in water at 25 °C, with values of 17 g/L and 18 g/L, respectively. Since the solubility of magnesium hydroxide in water is very low (0.009 g/L) at 25 °C, 1 g of magnesium hydroxide was used in 50 mL of solution. The synthesis was carried out in an autoclave provided by Parr Instrument Company (Moline, IL, USA) using a Model 4838 Reactor controller coupled to Model 4793 general-purpose pressure vessels with four valves. The synthesis scheme is reported in Figure 8.

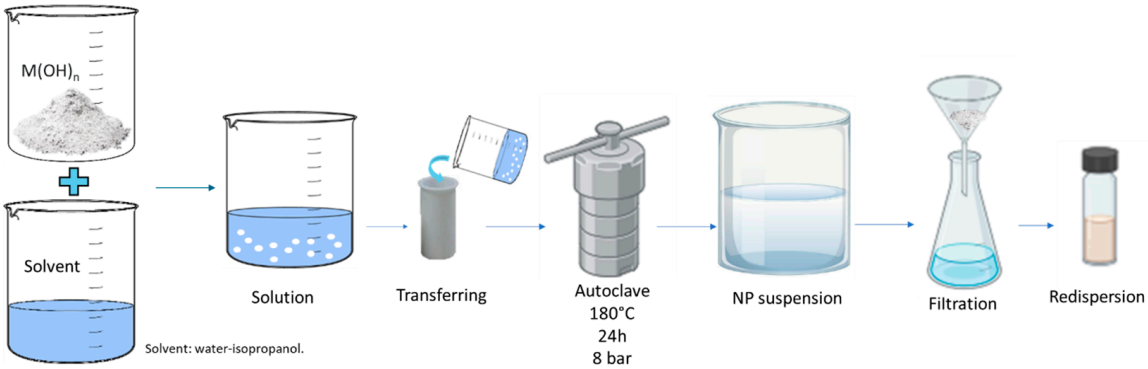

Figure 8. Synthesis scheme of hydroxides.

The preparation of the synthesis was carried out through the following phases:

1. Initial crushing: The micrometer-sized hydroxide particle grains were placed in a mortar and ground. This mechanical crushing process made it possible to reduce the particle size, increase their exposed surface area, and improve efficiency in subsequent steps.
2. Solvent dispersions: The ground particles were then dispersed in the solvents.
3. Autoclave treatment: The suspension of particles was transferred to the autoclave in a sealed container that can withstand high temperatures and pressures. The autoclave was heated at 180 °C and 8 bar for 24 h.
4. Evaluation of the stability of the system: Once the process was completed, a suspension of nanoparticles dispersed in the solvent was obtained. The resulting mixtures were thus sonicated in an ultrasonic bath for 30 min, collected via filtration, and dried at 60 °C overnight.
5. The nanoparticles were redispersed in the proper solvent.

3.3. Characterization

The *XRD patterns* were acquired by a Philips PW 1050/39 powder diffractometer in Bragg–Brentano geometry, which uses Cu Kα radiation (λ = 1.54056 Å) as the X-ray source. The X-ray tube is powered by a generator that works at a power of 40 KV and a current of 30 mA. XRD patterns were acquired in the range of 20° to 70° (2θ) with a step of 0.05° and an acquisition time for each step of 5 s. Identification of mineralogical phases was performed using X'pert HighScore® software.

The *FT-IR spectra* were acquired with a Bruker VERTEX 70V FTIR spectrophotometer with a Platinum ATR accessory (diamond crystal) in the spectral range of 4000–400 cm^{-1}, using a step of 2 cm^{-1} and averaging over 120 scans at 2 hPa. The data analysis was performed using OPUS 7.5® software.

The *optical microscope images* were captured using an Optika optical microscope equipped with an integrated 5-megapixel digital camera, ensuring high-resolution imaging and accurate documentation. The microscope featured objective lenses with magnification levels of 4×, 10×, 40×, and 100×, allowing for detailed analysis across multiple scales.

For the morphological and dimensional analysis of the synthesized nanoparticles, a Phenom Pro X *scanning electron microscope (SEM)* (Thermo Fisher Scientific, Waltham, MA, USA) was used. The SEM was operated at accelerating voltages of 15 kV, allowing for magnifications between 500× and 13,500×. The instrument was equipped with an Energy Dispersive X-ray Spectroscopy (EDS) detector supplied by Alfates, which allowed for compositional analysis. Samples were imaged digitally using transmission electron microscopy (TEM). Images and EDX spectra were acquired using a Tecnai G2 F20 X-TWIN (FEI, Eindhoven, The Netherlands, 2011) microscope with a Schottky-type field emission

electron source, a high-angle annular dark field (HAADF) detector, a single- and double-tilted sample holder, and an 11MPix ORIUS SC1000B (Gatan) CCD camera. Samples were mounted directly on a holey carbon-coated copper grid (Agar Scientific Ltd., Stansted, UK).

The crystalline structure was determined with a *Transmission Electron Microscope* (TEM) working in diffraction mode, while for micrographs, an objective aperture was additionally inserted for enhanced contrast.

The surface areas of the produced materials were examined by conducting *nitrogen gas adsorption* via the BET (Brunauer–Emmet–Teller) method using a surface area and porosity analyzer, TriStar II 3020 (Micromeritics, USA). Prior to these measurements, each sample was degassed for 1.5 h at 120 °C under nitrogen flow using the FlowPrep 060 sample degas system (Micromeritics, USA).

4. Conclusions

The hydrothermal synthesis performed in an autoclave, using a solvent mixture of 75% water and 25% isopropanol at 180 °C for 24 h, has proven to be a highly effective and reproducible method for producing stable and well-dispersed nanoparticles of barium, strontium, and magnesium hydroxides. The optimized solvent composition favored uniform suspensions with limited particle aggregation. This one-pot method yielded nanoparticles with distinct morphologies. Acicular and fibrous morphologies were obtained for $Ba(OH)_2$ and $Sr(OH)_2$, while $Mg(OH)_2$ formed spheric and hexagonal structures. The simplicity and environmental compatibility of this method make it a promising strategy for the sustainable production of functional nanomaterials, with potential applications in advanced technological fields.

Author Contributions: M.L.S. and D.F.C.M.: Conceptualization and methodology, writing—review and editing. C.T.: Synthesis, XRD patterns and FT-IR spectra, writing. F.A.: SEM and MO investigation. R.S.: TEM and gas adsorption. D.F.C.M.: Funding. All authors have read and agreed to the published version of the manuscript.

Funding: This research work is supported by the MUR-PNRR SAMOTHRACE Project (ECS00000022). F.A. thanks MIUR for the Project PON Ricerca e Innovazione 2014–2020—Avviso DD 407/2018 "AIM Attrazione e Mobilità Internazionale" (AIM1808223).

Institutional Review Board Statement: Not applicable.

Informed Consent Statement: Not applicable.

Data Availability Statement: The datasets generated and/or analyzed during the current study are available from the corresponding author on reasonable request.

Acknowledgments: SEM investigations were performed at the ATEN-Center of University of Palermo.

Conflicts of Interest: The authors declare no conflicts of interest.

References

1. Gleiter, H. Nanostructured Materials: Basic Concepts and Microstructure. *Acta Mater.* **2000**, *48*, 1–29. [CrossRef]
2. Rao, C.N.R.; Müller, A.; Cheetham, A.K. *The Chemistry of Nanomaterials: Synthesis, Properties and Applications*; John Wiley & Sons, Ltd.: Weinheim, Germany, 2004; pp. 1–20. ISBN 978-3-527-60247-6.
3. Mohajerani, A.; Burnett, L.; Smith, J.V.; Kurmus, H.; Milas, J.; Arulrajah, A.; Horpibulsuk, S.; Abdul Kadir, A. Nanoparticles in Construction Materials and Other Applications, and Implications of Nanoparticle Use. *Materials* **2019**, *12*, 3052. [CrossRef]
4. Fathi-Achachelouei, M.; Knopf-Marques, H.; Ribeiro da Silva, C.E.; Barthès, J.; Bat, E.; Tezcaner, A.; Vrana, N.E. Use of Nanoparticles in Tissue Engineering and Regenerative Medicine. *Front. Bioeng. Biotechnol.* **2019**, *7*, 113. [CrossRef]
5. David, M.E.; Ion, R.-M.; Grigorescu, R.M.; Iancu, L.; Andrei, E.R. Nanomaterials Used in Conservation and Restoration of Cultural Heritage: An Up-to-Date Overview. *Materials* **2020**, *13*, 2064. [CrossRef]

6. Abid, N.; Khan, A.M.; Shujait, S.; Chaudhary, K.; Ikram, M.; Imran, M.; Haider, J.; Khan, M.; Khan, Q.; Maqbool, M. Synthesis of Nanomaterials Using Various Top-down and Bottom-up Approaches, Influencing Factors, Advantages, and Disadvantages: A Review. *Adv. Colloid Interface Sci.* **2022**, *300*, 102597. [CrossRef]
7. Sabatier, P.A. Top-Down and Bottom-Up Approaches to Implementation Research: A Critical Analysis and Suggested Synthesis. *J. Public Policy* **1986**, *6*, 21–48. [CrossRef]
8. Jasti, R.; Bertozzi, C.R. Progress and Challenges for the Bottom-up Synthesis of Carbon Nanotubes with Discrete Chirality. *Chem. Phys. Lett.* **2010**, *494*, 1–7. [CrossRef] [PubMed]
9. Amendola, V.; Meneghetti, M.; Granozzi, G.; Agnoli, S.; Polizzi, S.; Riello, P.; Boscaini, A.; Anselmi, C.; Fracasso, G.; Colombatti, M.; et al. Top-down Synthesis of Multifunctional Iron Oxide Nanoparticles for Macrophage Labelling and Manipulation. *J. Mater. Chem.* **2011**, *21*, 3803–3813. [CrossRef]
10. Balducci, G.; Diaz, L.B.; Gregory, D.H. Recent Progress in the Synthesis of Nanostructured Magnesium Hydroxide. *CrystEngComm* **2017**, *19*, 6067–6084. [CrossRef]
11. Wu, J.; Yan, H.; Zhang, X.; Wei, L.; Liu, X.; Xu, B. Magnesium Hydroxide Nanoparticles Synthesized in Water-in-Oil Microemulsions. *J. Colloid Interface Sci.* **2008**, *324*, 167–171. [CrossRef]
12. Giorgi, R.; Bozzi, C.; Dei, L.; Gabbiani, C.; Ninham, B.W.; Baglioni, P. Nanoparticles of $Mg(OH)_2$: Synthesis and Application to Paper Conservation. *Langmuir* **2005**, *21*, 8495–8501. [CrossRef]
13. Giorgi, R.; Ambrosi, M.; Toccafondi, N.; Baglioni, P. Nanoparticles for Cultural Heritage Conservation: Calcium and Barium Hydroxide Nanoparticles for Wall Painting Consolidation. *Chem.–A Eur. J.* **2010**, *16*, 9374–9382. [CrossRef]
14. Ciliberto, E.; Condorelli, G.G.; La Delfa, S.; Viscuso, E. Nanoparticles of Sr(OH)2: Synthesis in Homogeneous Phase at Low Temperature and Application for Cultural Heritage Artefacts. *Appl. Phys. A* **2008**, *92*, 137–141. [CrossRef]
15. Gan, X.Y.; Jayatissa, A.H.; Yu, Z.; Chen, X.; Li, M. Hydrothermal Synthesis of Nanomaterials. *J. Nanomater.* **2020**, *2020*, 8917013. [CrossRef]

Disclaimer/Publisher's Note: The statements, opinions and data contained in all publications are solely those of the individual author(s) and contributor(s) and not of MDPI and/or the editor(s). MDPI and/or the editor(s) disclaim responsibility for any injury to people or property resulting from any ideas, methods, instructions or products referred to in the content.